Ocean Engineering 277 (2023) 114224

Contents lists available at ScienceDirect

Ocean Engineering

journal homepage: www.elsevier.com/locate/oceaneng

Towards uncertainty and sensitivity analysis for modal parameters identification during ice–structure interaction

Chunlin Wang [a,*], Torodd Skjerve Nord [a], Gesa Ziemer [b], Guoyuan Li [a]

[a] Department of Ocean Operations and Civil Engineering, Norwegian University of Science and Technology, 6009 Ålesund, Norway
[b] Institute for Maritime Energy Systems, DLR, Geesthacht, Germany

ARTICLE INFO

Keywords:
Uncertainty analysis
Sensitivity analysis
SSI-cov
Ice–structure interactions
Modal parameter identification

ABSTRACT

The integrity of offshore structures is prone to the threat of drifting sea ice. By exciting the natural frequencies of the ice–structure interaction system, severe vibrations may occur. For a better understanding of how dynamic ice–structure interaction affects the system properties, a stochastic subspace system identification technique, SSI-cov is introduced to identify modal parameters during dynamic ice–structure interactions. Due to the uncertain input variables of SSI-cov, the identified modal parameters suffer from the quantitative judgment of the analyst. To address this problem, this study proposes an uncertainty analysis (UA) framework to obtain estimates of modal parameters. This framework constitutes both a sensitivity analysis (SA) and a UA. First, SA is applied to pick up the input variables that contribute the most to the identified modal parameters. Next, the important variables are left free to vary over their range of existence to obtain the modal parameters' uncertainties. The framework is applied to full-scale tests from Norströmsgrund lighthouse and model tests carried out in Hamburg Ship Model Basin (HSVA). The comparison with traditional automated modal parameter identification shows its superiority in terms of the accuracy of modal parameters.

1. Introduction

The integrity of a structure located in ice-infested waters is prone to the threats of ice forces and ice-induced vibrations. Substantial efforts were made to understand both the physical processes leading to ice-induced vibrations (IIVs), based on observations, measurement campaigns on lighthouses, bridge piers, and oil platforms for decades, but also model scale tests in ice basins (Nord et al., 2019). Drifting ice may cause various modes of ice–structure interaction, in which some lead to more severe vibrations than others, such as for instance crushing failure mode leading to frequency lock-in vibrations (FLI). This mode is particularly violent with respect to ice forces and structural responses, some examples in full scale with threats of the structural integrity (Jefferies, 1988; Blenkarn, 1970). IIVs are often associated with crushing failure, and IIVs are also shown to pose a threat to the structural integrity as well (Blenkarn, 1970).

While much attention naturally has been made to come up with phenomenological models to predict IIVs, a very limited number of studies were made to seek fundamental system parameters of the underlying mechanical system by means of system identification. For structures exposed to wind and waves, system identification has provided unique insight into how the system properties change for different properties of the wind or wave characteristics. For ice–structure interaction systems, some work on model-scale experiments was conducted by Singh et al. (1990), while on Full-scale, Nord et al. applied SSI-cov to identify modal parameters on the Norströmsgrund lighthouse under a variety of ice–structure interaction modes (Nord et al., 2019). Level ice acting on a vertically-sided structure may fail to generate different failure modes depending on indentation velocity, aspect ratio, and ice properties (Timco, 1991). In Fig. 1, crushing failure Fig. 1(a) represents the deformation and failure of ice at high indentation speeds and low aspect ratios. It results from the non-simultaneous occurrence of high-pressure zones across the ice–structure interface (Nord et al., 2017). The crushing failure mode is mostly associated with IIVs and the main ice failure mode in our experiment (Hendrikse and Nord, 2019). Other failure modes, such as bending failure Fig. 1(b), splitting failure Fig. 1(c), buckling failure Fig. 1(d), and pushing floes Fig. 1(e) are not considered in this paper and can be referred to Kärnä and Jochmann (2003). The understanding of how ice failure modes change the modal parameters of the structure is beneficial to the structural safe design. However, it is still challenging in the research field for safe design and accurate predictions in fatigue assessments.

To this end, Operational Modal Analysis (OMA) was proposed to estimate the modal parameters from measurements of the vibration response only (Rainieri and Fabbrocino, 2014). It can be implemented

* Corresponding author.
E-mail address: chunliw@ntnu.no (C. Wang).

https://doi.org/10.1016/j.oceaneng.2023.114224
Received 7 January 2023; Received in revised form 3 March 2023; Accepted 14 March 2023
Available online 30 March 2023

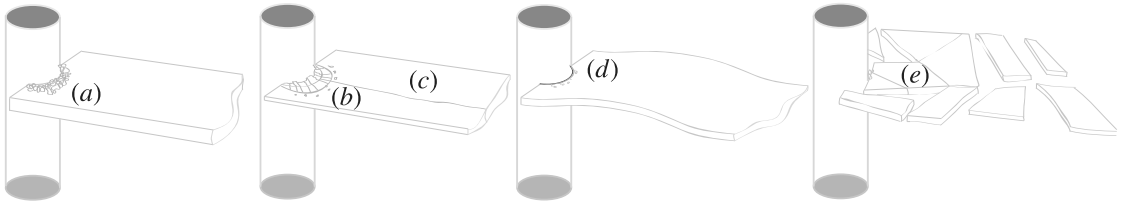

Fig. 1. The different types of failure modes in ice–structure interaction (Nord et al., 2017).

efficiently, economically, and safely, and does not interfere with the normal use of the structure. The identified modal parameters are representative of the actual behavior of the structure since it takes advantage of natural excitation instead of artificial excitation. The most popular OMA method is the Stochastic Subspace Identification (SSI) method since it offers high accuracy in the identification of closely-spaced modes and is especially suited to be automated (He et al., 2021). SSI is to identify physical modes by picking up stable poles in a stability diagram. Since the estimated modal parameters are afflicted with statistical uncertainty, an efficient multi-order uncertainty computation method, called covariance-based SSI (SSI-cov), was proposed to estimate the variance of the identified modal parameters (Döhler and Mevel, 2013). Due to its low computational cost and high identification accuracy, it has been widely applied to analyze the parameters of structures in recent years.

Although SSI-cov can effectively remove modes with large variances to obtain physical modes, its accuracy of modal parameter identification cannot be guaranteed due to various assumptions and uncertain input parameters. For example, ice forces usually cannot be represented as Gaussian white noise and therefore the input violates the random white noise assumption of SSI-cov. In addition, the structure is described as a linear time-invariant system. Such assumptions could result in errors in the modal parameters identification. Besides that, SSI-cov contains many uncertain input parameters such as slack values, stability criterion, system orders, etc. The parameters' uncertainty is propagated to the identified parameters and results in the poor estimation of their values. To reduce the uncertainty of slack values, clustering technologies were introduced for automated OMA (Reynders et al., 2012). Clustering approaches can implement parameter identification in an automatic way and avoid the artificial selection of slack values. Nevertheless, clustering algorithms will bring additional uncertainties as they contain several uncertain parameters and algorithm structure uncertainty (known as model uncertainty). As a consequence, a robust outlier detection was proposed to reduce statistical uncertainty caused by the clustering algorithm (Zeng and Hoon Kim, 2021). However, it cannot remove the algorithm uncertainty completely. In addition, clustering technologies did not consider the uncertainty from other input parameters of SSI-cov. Therefore, it is significant to investigate how the identified parameters' values vary under the different sources of input variables' uncertainty, which could ensure more convincing parameter estimation for engineers.

To improve the accuracy of SSI-cov identification, this research proposed a modal parameters analysis framework based on UA and sensitivity analysis (SA). SA aims to pick up those factors that account for the most contributions to the model output. That is beneficial to lower the burden of UA caused by large amounts of variables. The main contributions are as follows: (1) SA is introduced to remove unimportant input parameters of SSI-cov; (2) Sihouette and robust outlier detection are used to improve the robustness of clustering algorithm for automated OMA; (3) UA is applied on several ice–structure interaction datasets for precise parameters identification. The analysis results could provide support for structural health monitoring (SHM) of offshore structures.

The whole paper is structured as follows. Section 2 presents related work regarding automated OMA approaches and UA in other fields. Section 3 gives an introduction on the proposed analysis framework and corresponding algorithms. In the next section, several case studies are shown to verify the feasibility of the proposed method.

2. Related work

Safe design of the deployed offshore structures requires understanding the ice-induced vibrations as a result of level ice interacting with a vertically-sided structure (Kärnä et al., 2013). To obtain knowledge of the dynamic behavior of the structure, OMA is introduced to analyze structure modes, each one characterized by a set of parameters (natural frequency, damping ratio, model shape). As uncertainty is intrinsic in various identification algorithms, it is of importance to evaluate the uncertainty in the identified parameters. This section mainly introduces the development of OMA and uncertainty evaluation and explores how to apply UA for better OMA of offshore structures.

2.1. Operational modal analysis

Before the wide application of OMA, experimental modal analysis (EMA) played a pivotal role in parameter identification. However, EMA techniques cannot be applied to analyze massive structures and a system in operational condition because the power of the device is insufficient to excite the structure to attain the required magnitude (Lauwagie et al., 2006). For this reason, OMA was developed to estimate modal parameters based on the data collected when the structure is under the operational conditions (Zahid et al., 2020). The identified parameters can be representative of the actual behavior of the structure.

SHM requires real-time parameters analysis to perform fault detection. Unfortunately, much user intervention on modal parameters analysis is an obstacle in a real application (Zeng and Hoon Kim, 2021). In recent years, growing attention has been put on automated OMA. Many system identification algorithms have been developed to identify system modes. Yang et al. developed an automated OMA based on an eigensystem realization algorithm and a two-stage clustering strategy. It can estimate modal parameters effectively in real-time (Yang et al., 2019). Magalhaes et al. applied the poly-Least Squares Complex Frequency Domain method to perform online parameters identification (Magalhaes et al., 2009). Au et al. combined the Bayesian method with a fast Fourier transform of ambient data (Au, 2011). It can meet the requirement of real-time parameters analysis as Bayesian modal identification can be performed in a few seconds. Reynders et al. introduced uncertainty bounds on the modal parameters estimated with SSI (Reynders et al., 2008). The proposed method can estimate the variance of modes from a single measurement record. Due to the time-consuming variance estimation of parameters, Döhler et al. proposed an efficient multi-order uncertainty computation approach (SSI-cov) (Döhler and Mevel, 2013). Among these approaches, SSI-cov is the most popular method since it offers high accuracy in the identification of closely-spaced modes and is especially suitable to be automated (He et al., 2021). Therefore, it has been widely used for model parameters identification of ice–structure interaction in Nord et al. (2019), flexible spacecraft in Xie et al. (2016), large-scale bridge in Pan et al. (2021), and so on.

After SSI analysis, poles at different orders are obtained and form a stabilization diagram. Next, the slack value is used to pick up the stable poles that are representative of the physical modes. The stable poles form multiple vertical lines in the diagram that are regarded as physical modes (Nord et al., 2019). Due to the limitation of many

parameters selection, several strategies have been proposed for automatic physical mode identification. Hierarchical clustering was proposed based on eigenfrequency difference and the modal assurance criteria (MAC) value as distance measures (Pappa et al., 1998). Afterwards, Goethals et al. incorporated the eigenfrequency and damping ratio difference into the Hierarchical clustering algorithm. Closely-spaced modes are grouped into the same cluster, they are then separated by the MAC value. In addition to Hierarchical clustering, K-means, and fuzzy C-means are employed to find physical modes as well (Mao et al., 2019; He et al., 2021). However, clustering results are sensitive to the user-defined number of clusters. To address this limitation, Density-based spatial clustering of applications with noise (DBSCAN) was proposed to cluster physical modes (Ye and Zhao, 2020; Li et al., 2020). In recent work, Kvaale et al. proposed hierarchical DBSCAN (HDBSCAN) for automated parameter identification since it requires fewer parameters (Kvåle and Øiseth, 2021).

Although the aforementioned clustering techniques achieve better performance on mode identification, they cannot remove estimating errors caused by parameter uncertainty. Therefore, it is necessary to make an uncertainty evaluation during automated OMA to obtain more convincing results.

2.2. Uncertainty analysis

In order to obtain accurate model parameters, SSI-cov uses stabilization criteria to remove part of bias of the model and the modes, and slack values to remove artificial modes with large variances (Reynders et al., 2008). However, it cannot remove or quantify other uncertainties such as the number of data samples and parameters' values. In addition, stabilization criteria and slack values bring more uncertain parameters.

To reduce the impact of slack values on stable poles selection, Hierarchical clustering is used to replace slack values-based method for clustering physical modes (Wang et al., 2022). However, uncertainties induced by other parameters are not considered. Therefore, this study introduces UA to quantify uncertainties caused by uncertain input parameters.

UA aims to provide confidence that model-based decisions are robust to underlying uncertainties. Uncertainties are mainly divided into two categories: aleatory uncertainty and epistemic uncertainty. Aleatory uncertainty arises from physical phenomena that are random by nature. It is extremely hard to quantify and eliminate aleatory uncertainty during modeling calibration. In contrast to aleatory uncertainty, epistemic uncertainty concern the model parameters and model discrepancy, also known as parametric uncertainty and structural uncertainty. Epistemic uncertainty can be reduced when better knowledge of the model structure and more accurate data become available (Xiao and Cinnella, 2019). Therefore, the main concern of this study is to investigate the epistemic uncertainty of quantities of interest (QoI).

Uncertainty quantification (UQ) aims to quantify the uncertainty of QoI that is induced by propagating uncertain random variables to the model output. There are many technologies that are developed for UQ, for instance, SA, Monte Carlo simulation, response surface approaches, evaluation of classical statistical confidence bounds, Dempster-Shafer theory, and Bayesian inference (Zhang et al., 2020). They are widely applied to various domains such as Deep Learning, medical health, environmental science, material science, modal parameter identification, etc. For example, Dusenberry et al. analyzed RNN model uncertainty for electronic health records (Dusenberry et al., 2020). Various Bayesian RNNs were introduced to place priors on different subsets of the parameters to determine the level of the model. Hu et al. presented the Markov Chain Monte Carlo (MCMC) algorithm to quantify the parameter uncertainty that arises from the modeling of macro-fiber composite materials (Hu et al., 2014). The study extended a data-driven deterministic estimation technique, presented in Hu et al. (2012) that was used to obtain the unknown model parameters, to investigate the parameter uncertainty that fits into non-Gaussian distributions. In order to improve the accuracy of modal parameters identification, SSI-cov was proposed to estimate the variance of modal parameters (Reynders et al., 2008). Due to the high computational cost of SSI-cov, Döhler et al. delivered an efficient multi-order uncertainty computation for SSI-cov (Döhler and Mevel, 2013). This improved SSI-cov is both computationally and memory efficient. However, parametric uncertainty still exists as SSI-cov only estimates the structural uncertainties from SSI algorithm.

It is challenging for UQ since a large number of simulations are required. Specifically, SSI-cov needs to conduct singular-value decomposition to obtain system matrices, which is extremely time-consuming. Therefore, in this study, SA is introduced to reduce the burden of UQ. SA is to study how the variation of QoI is apportioned to the model inputs. After SA, those important variables can be picked up for the following UQ. The detailed description regarding SA can be found in review papers (Zhang et al., 2020; Saltelli et al., 2019; Razavi et al., 2021).

3. Method

This section is to introduce the proposed UA framework that is applied to identify modal parameters. Compared with traditional OMA, it can estimate the uncertainty bound of parameters induced by uncertain input variables. As shown in Fig. 2, the framework is mainly divided into three parts. The first part is to do a model evaluation based on the input parameters sampled from a hypothetical distribution. The second one is automatic parameter identification using the clustering method. The identified modal parameters are used for the following sensitivity analysis and uncertainty analysis. The workflow is first conducting SA to select the most important input variables, second doing UA based on the selected uncertain variables.

3.1. Model evaluation

Model evaluation is to make simulations based on experimental settings. It is the core and most time-consuming part of UA and SA. UQ involves determining the probability distributions of each input variable. Generally, the probability distribution function (PDF) is inferred based on experimental data or thumb rules. The PDF indicates the whole range of parameters' uncertainties. An accurate PDF estimation is extremely hard because of the limited data samples.

In general, all parameters are assumed to be independent and subject to certain distributions (uniform or normal). In order to represent the PDF, two hyperparameters (μ *and* σ) are introduced to control the uncertainty across all parameters (Pathmanathan et al., 2019). The PDF is defined as shown in Eqs. (1) and (2):

$$p \sim N(\mu, \sigma^2) \tag{1}$$

where 'N' denotes normal distribution.

$$p \sim U(\mu - \sigma, \mu + \sigma) \tag{2}$$

where 'U' represents uniform distribution.

The assumption of PDF has a significant influence on the identified results. If PDF is assumed a normal distribution, some data are sampled from the tail of the normal distribution. These data might exceed the reasonable range of the parameter's value, leading to an error in SSI-cov analysis. To avoid this problem, the uniform function is chosen as the distribution function of parameters since it can define the minimum and maximum value of the parameter's range. After the PDF is determined, the random samples are obtained by Latin-hypercube sampling (LHS). Compared with Monte Carlo sampling, LHS can sample data across the whole space of parameters, and hence it is effective in SA with small samples (Helton and Davis, 2003). The random samples and the measured structural response are fed into the SSI-cov to compute modal parameters. The simulations will be repeated by as many times as the

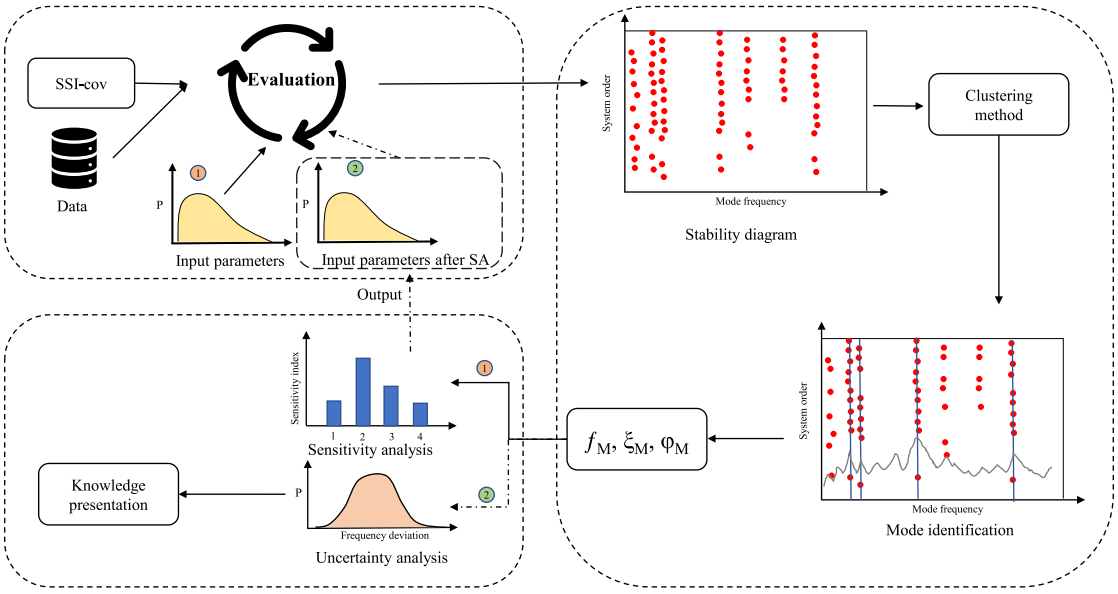

Fig. 2. The framework of uncertainty analysis and sensitivity analysis on modal parameters identification.

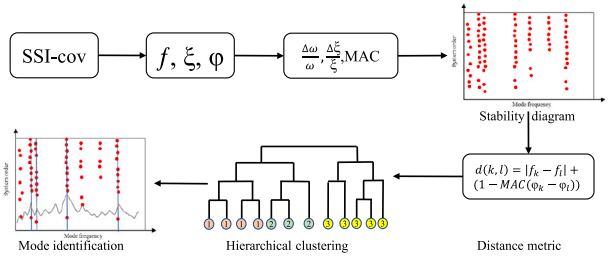

Fig. 3. The schematic diagram of mode identification using Hierarchical clustering.

size of the samples. Finally, the sensitivity of inputs on QoI is computed based on simulated results.

The model evaluation will be carried out two times. The first time is for SA to pick up the influential input factors and the second time is for UA when the selected factors are applied for SSI-cov to identify modal parameters under different ice failures and ice velocities.

3.2. Modal parameters identification

After model evaluation, the obtained parameters (eigenvalues and eigenvectors) are used to compute modal parameters ($f, \xi, and\ \varphi$). Next, modal parameter identification is carried out to obtain physical modes. The schematic diagram of modal parameter identification is shown in Fig. 3.

First of all, stable poles are picked up based on the stability criterion to form a stability diagram. The stability criterion involves the tolerance deviances to frequency ($\frac{\delta\omega}{\omega}$), damping ($\frac{\delta\xi}{\xi}$), and MAC-values, as well as the normalized standard deviation of the frequency ($\hat{\sigma}_{\omega_i}/\omega_i$). The pole is taken as stable if its stability parameters fulfill the pre-defined criterion.

After stable poles are obtained, a clustering algorithm is introduced to identify modes from these stable poles. In this study, a Hierarchical clustering algorithm is applied to identify modal parameters automatically. Compared with the slack value-based method, it has the advantage of higher accuracy and less human intervention (Wang et al., 2022). In addition, it has fewer parameters to determine, which can reduce the uncertainties of parameters. The distance metric in the Hierarchical clustering is selected as $d(k,l) = |f_k - f_l| + (1 - MAC(\varphi_k - \varphi_l))$. $d(k,l)$ represents the distance between mode 'k' and mode 'l'.

In order to eliminate uncertainties in the Hierarchical clustering algorithm, two strategies are employed to improve the robustness of the algorithm. The first method is to use the Silhouette value to evaluate the clustering results. It measures how similar a point is to points in its own cluster when compared to points in other clusters. The higher it is, the better the samples are clustered. The principle is shown in Eq. (3).

$$s(i) = \frac{b(i) - a(i)}{max(b(i), a(i))} \tag{3}$$

where b(i) denotes the average distance of point 'i' with all points in the closest cluster to its cluster; a(i) is the average distance of point i with other points in the same clusters; s(i) is the silhouette coefficient that ranges from [−1,1].

Due to the variability of modal estimates, outlier detection is used for penalizing undesirable modes in the final clusters to reduce identification uncertainties (Zeng and Hoon Kim, 2021). Eq. (4) defines the robust distance (RD).

$$RD(x) = d(x, \hat{\mu}_{MCD}, \hat{\mu}_{MCD}) \tag{4}$$

where MCD is the minimum covariance determinant that is used for outlying values detection. x represents frequency in this study; $\hat{\mu}_{MCD}$ denotes the MCD estimates of location; $\hat{\mu}_{MCD}$ is the covariance of MCD.

After that, a hierarchical tree could be created as shown in Fig. 3. The color of the leaves in the tree represents different clusters. If a cluster contains a pre-defined number of poles, the poles in this cluster render a physical mode as shown by the straight line in the stability diagram. After clustering, the stability diagram could show physical modes.

3.3. Uncertainty analysis and sensitivity analysis

Too many uncertain parameters lead to the high cost of UA. Therefore, SA is used to pick up the most sensitive parameters that contribute to the variation of the modal parameters. Global sensitivity analysis (GSA) is a powerful tool to estimate the total sensitivity of all factors. In this study, two popular GSA approaches are chosen to conduct SA. They are the variance-based Sobol method (Sobol, 2001) and cumulative distribution function (CDF)-based PAWN method (Pianosi and Wagener, 2015).

A generic model is described as follows.

$$Y = f(X_1, X_2, \ldots, X_M) \tag{5}$$

Table 1
The main test runs and the corresponding parameters settings.

Run	Model	Ice type	Ice drift velocity	Ice thickness	Flexural strength
32010	9500 MDOF	Model ice	4–150 mm/s	41 mm	56 kPa
25010	9200 MDOF	ICMI	4–150 mm/s	23 mm	86 kPa

where Y is the model output of interest; $\mathrm{X}=(X_1, X_2, \ldots, X_M) \in \mathbb{R}^{M\times 1}$ is the model input which contains M factors; $f(X)$ can represent abstract models (data-driven models, mathematical model, or defined function) and mechanical models (robots). In this study, $f(X)$ corresponds to SSI-cov and Hierarchical clustering methods.

Sobol's method is based on the total variance decomposition.

$$V(Y) = \sum_{i=1}^{M} V_i + \sum_{i=1}^{M-1}\sum_{j=i+1}^{M} V_{ij} + \cdots + V_{1,\ldots,M} \tag{6}$$

where $V(Y)$ is the variance of model output Y; V_i is the variance contribution of X_i to the model output; V_{ij} is the variance from the interaction between X_i and X_j; $V_{1,\ldots,M}$ represents the variance induced by the interaction between M parameters. The V_i is addressed as the first-order or main effect of X_i on Y. Therefore the first-order sensitivity index (S_i) of X_i is computed by Eq. (7). The total sensitivity index (S_{Ti}) is obtained by Eq. (8).

$$S_i = \frac{V_i}{V(Y)} \tag{7}$$

$$S_{Ti} = \frac{V_i + V_{ij} + \cdots + V_{1,\ldots,M}}{V(Y)} = 1 - \frac{V_{\sim i}}{V(Y)} \tag{8}$$

where $V_{\sim i}$ represents the total variance contribution of remaining parameters to Y given X_i. The detailed description can be referred to Saltelli et al. (2008).

'PAWN' is a CDF-based GSA method. The main principle is to estimate the difference between unconditional CDF and conditional CDF using Kolmogorov–Smirnov (KS) test.

$$\begin{cases} \hat{S}_i = \max\limits_{k=1,\ldots,M} KS(I_k) \\ KS(I_k) = \max\limits_{y} |F_y(y) - F_{y|\tilde{x}_i}(y|\tilde{x}_i \in I_k)| \end{cases} \tag{9}$$

where KS is Kolmogorov–Smirnov statistic; $F_y(y)$ is unconditional CDF where $y \subseteq Y$ and $F_{y|\tilde{x}_i}(y|\tilde{x}_i \in I_k)$ is conditional CDF where $\tilde{x}_i$ is fixed. The detailed information can be found in Pianosi and Wagener (2015).

The flowchart of the two SA methods is shown in Fig. 4. First of all, some variables are defined manually. 'N' is the size of Sobol's sample. 'M' is the number of parameters in modal parameters identification. 'Unif' assumes the distribution function is uniform. 'LHS' is a sampling strategy. 'NU' is the size of unconditional samples while 'NC' is the size of conditional samples. 'n' is the conditional point from which conditional samples are sampled. Next, different sampling methods are applied to generate different data samples. 'XA' is the sampled data that is used to estimate 'YA' through model evaluation while 'XB' is used to compute 'YB'. Likewise, 'XU' is to estimate 'YU' and 'XX' is to obtain 'YC'. After that, 'YA' is used to estimate V_i by the Sobol method while 'YB' is employed to estimate $V_{\sim i}$. 'YU' is to obtain $F_y(y)$ while is to get $F_{y|\tilde{x}_i}$. Followed by Sobol and PAWN analysis, two sets of SA results can be obtained. They are compared to obtain convincing sensitivities of all parameters. After important parameters are picked, LHS sampling is used to generate a sample, and Model evaluation is conducted to carry out UQ of identified modal parameters. The two approaches are integrated into a MATLAB toolbox in Pianosi et al. (2015).

4. Case study

4.1. Data collection

Ice–structure interaction data are collected from model-scale experiments and full-scale experiments. All model-scale tests are carried out in the Hamburg Ship Model Basin's (HSVA) large ice model basin.[1] The experiment setup was designed with a flexible foundation with adjustable mass and stiffness to mimic certain dynamic characteristics of the structure and a rigid model. Three Triax accelerometers are used to monitor the ice-induced vibrations of the structures in x- and y-direction (loading direction and perpendicular in-plane motion). The setup is shown in Fig. 5(a) (Stange et al., 2020). The data were collected under different structural and ice-related properties. The main tests and corresponding properties are shown in Table 1.

Different runs are designed with different global stiffness of the setup. Hydrodynamic added masses for models '9200' and '9500' are 16 kg and 19 kg separately. 'MDOF' represents the structure as multi-degree-freedom vibration which has two dominant frequencies (f_1 = 2.81 HZ and f_2 = 3.77 HZ). Ice types are HSVA's standard model ice and an improved crushing model ice (ICMI) (Ziemer et al., 2022). Model ice is generated by exposing the water surface to cooled air. The current model ice were not always ideal for crushing failure type of dynamic ice–structure interaction tests. Therefore, an alternative wave ice was proposed by simulating sea wave effects during water freezing. The first three test runs contain ice drift velocity from 4–150 mm/s whilst the ice velocity of '460101' starts from 14 to 150 mm/s. Based on different ice velocities, the measurements are grouped into different corresponding ice failure types (intermittent crushing (IC), frequency lock-in (FLI), and continuous crushing (CC). The full data set is described by Stange et al. (2020).

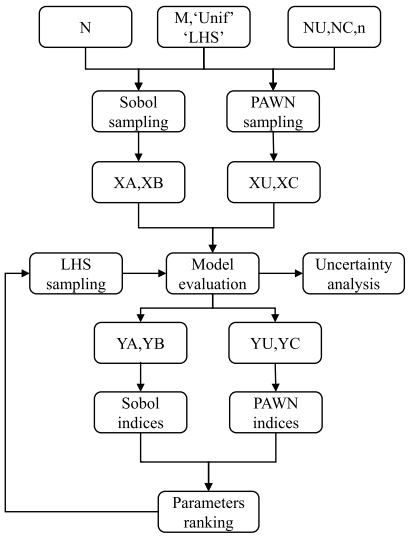

Fig. 4. The flowchart of Sobol and PAWN methods for sensitivity analysis.

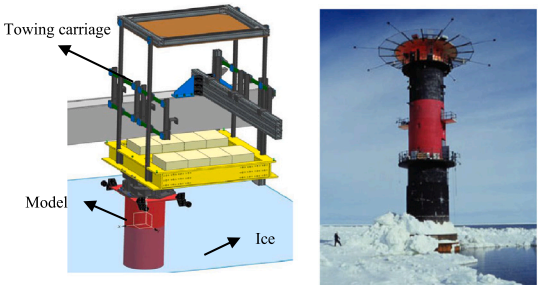

(a) Model-scale experiment (Ziemer et al., 2022)

(b) Full-scale experiment (Nord et al., 2019)

Fig. 5. The experiment setup for model-scale and full-scale tests.

[1] https://www.hsva.de/.

The full-scale experiments are conducted on the Norströmsgrund lighthouse which is located in the Gulf of Bothnia. As shown in Fig. 10, It is a gravity-based concrete structure with a wall thickness varying between 0.2 m at the top and 1.4 m at the mean water level (Nord et al., 2019). The diameter of the structure at the mean water level were 7.5 m at an elevation of +14.2 m . Nine panels were installed across the outer surface at the mean water level to measure the ice forces. Four accelerometers were equipped at different positions of the lighthouse. The detailed description can be found in Nord (2015), Nord et al. (2019).

4.2. Experiment setting

For sensitivity analysis, first of all, the sampling strategy and distribution function are selected as 'LHS' and uniform distribution. $\sigma = 40\% \times \mu$, where μ represents the predefined values of seven input parameters (Wang et al., 2022). Next, due to the time-consuming SSI-cov computation, it is not practical to set up a larger 'N'. Therefore, the Sobol index needs evaluation when 'N' is chosen as 2000. 'M' means 7 parameters, including the number of blocks (NB), block rows (BR), sampling frequency (SF), system order (SO), and stability criteria (the deviance in frequency (SC-I), the deviance in damping ratio (SC-II), and normalized standard deviation of the frequency (SC-III)). 'NU = 150', 'NC = 100', and 'n = 10' are referred to Pianosi and Wagener (2015). In Eq. (3), s is 0.5. As the first two modes (f_M, ξ_M, φ_M) are the modes in the model-scaled experiment that were designed to be easily excited by the ice force. Hence they are used for the output of interest in SA.

For UA, the sample size of uncertain parameters is 400. The benchmark values of the first and second natural frequencies are 21.35 and 29.52 (rad/s). SA is carried out using MATLAB toolbox (Pianosi et al., 2015). All MATLAB programs are run on the high-performance computer at the Norwegian University of Science and Technology (Själander et al., 2019).

4.3. Sensitivity analysis

Due to the desperately high time cost of model evaluations, several random cases are chosen for SA. For data file 32010, SA is applied for four different cases in which ice velocities are 14, 16, 18, and 20 (mm/s) separately. For data file 25010, ice velocities are from 18 to 26 (mm/s) with the step of 2 (mm/s). For full-scale measurements, ice velocities vary from 30 to 200 (mm/s).

Fig. 6 shows an example of how to use SA to pick up important factors. This figure plots the importance of seven factors to the first natural frequency when ice velocity is 20 mm/s. The blue squares are assumed indices with equivalent importance around 0.143. The PAWN index of SF is the largest at around 0.42. It is followed by BR at around 0.25. These two factors are to determine data size and input matrix for SSI-cov analysis. Hence, they have a very large influence on the identified frequencies. PAWN index ranks three around 0.21. That means the first frequency is impacted by the number of SO. However, when SO attains a certain value, the first frequency does not change anymore. Three stability criteria and NB account for a small contribution (from 0.1 to 0.17) to the variation of the first natural frequency. This is possibly because NB does not affect the eigenvalues, but only affects the results through the stabilization criterion. They can be removed from the set of uncertain input parameters. In other words, they are fixed at constant values in the following UA.

Fig. 7 presents statistics of parameters' PAWN indices among different velocities 14, 16, 18, 20 mm/s while parameters' Sobol indices are shown in Fig. 8. In both figures, the box represents the quantiles of parameters' sensitivity on the first and second natural frequencies. The PAWN indices of BR and SF are larger than the remaining overall. Therefore, BR and SF are chosen as uncertain factors for UA on data file 32010. In addition, for different cases, PAWN indices of different parameters have small variations. Nevertheless, in Fig. 8, Sobol indices

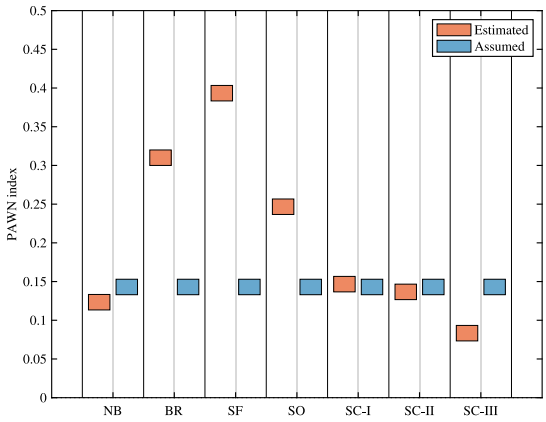

Fig. 6. The PAWN indices of seven input parameters on the first natural frequency when ice velocity is 20 mm/s.

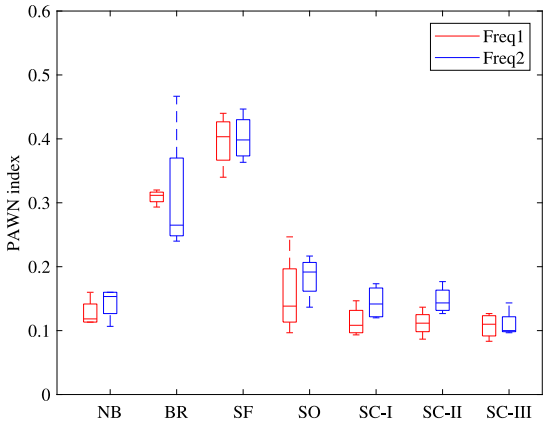

Fig. 7. The statistics of PAWN indices of seven parameters for different ice velocities in data file 32010.

of parameters vary drastically and are hard to rank. Therefore, the PAWN method has better performance regarding SA of parameters for ice–structure interaction analysis.

Fig. 9 shows the PAWN indices of BR and SF are the largest, varying from 0.25 to 0.55. The PAWN indices of the remaining parameters are below 0.2. Hence, BR and SF are chosen as uncertain factors for UA on data file 25010.

Fig. 10 shows the top two sensitive parameters are BR and SF whose PAWN indices are around 0.4 and 0.35 separately. Their indices are a bit smaller than the result in data files 32010 and 25010. This is possibly caused by the larger noise from the full-scale experiment in the real world.

To sum up, the most influential parameters are chosen as BR and SF for the following UA on data files 32010, 25010, and the full-scale experiment.

4.4. Uncertainty analysis

Table 2 lists the statistics of the identified first two natural frequencies. The statistics include mean value (Mean), standard deviation (Std), upper bound of 95% confidence interval (Upper), and lower bound of 95% confidence interval (Lower). The bold number means the correct identification. For the identified first natural frequency, the proposed method fails to identify it when ice failure is IC. Hence, it is not discussed in the following analysis. After the ice failure mode changes to FLI, the first natural frequencies are 19.84, 29.76, and 23.53 rad/s when ice velocities are 8, 10, and 20 mm/s, respectively. The

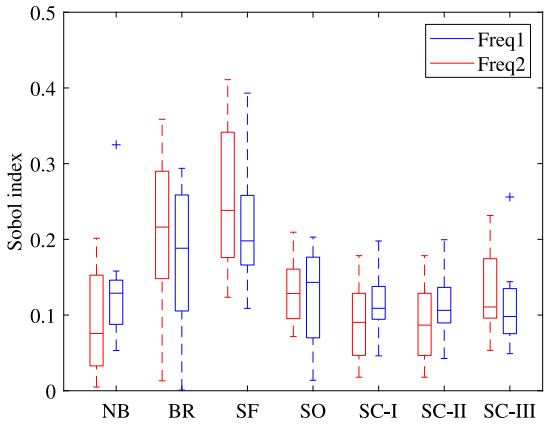

Fig. 8. The statistics of Sobol indices of seven parameters for different ice velocities in data file 32010.

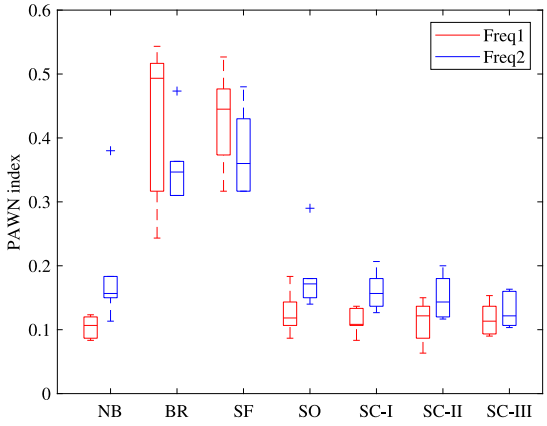

Fig. 9. The statistics of PAWN indices of seven parameters for different ice velocities in data file 25010.

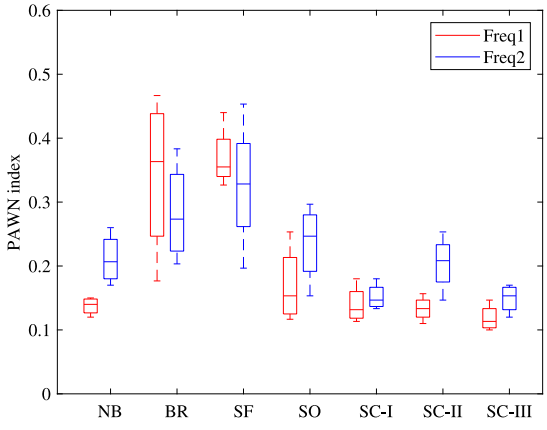

Fig. 10. The statistics of PAWN indices of seven parameters for different ice velocities in the full-scale test.

frequencies in the remaining cases are around 21.5 which is close to the benchmark value. In contrast to the first natural frequency, the second frequency identification becomes more intractable. 5 out of 15 identified second frequencies are over 30. One is less than 29, around 26.66 rad/s. Other frequencies can be identified correctly.

As to uncertainties of the identified frequencies, it is represented by the 95% confidence interval which is computed by '$Mean \pm 1.96 \times Std$'. The uncertainty explains the possible values of the identified parameters. In Table 2, the lower bound of the first frequency is −7.38 when ice velocity is 4 (mm/s). This value is obtained by statistical analysis. However, it cannot be less than zero in practice. When ice velocities are 12, 18. 28, and 65 (mm/s), the standard deviation of the identified first frequency is less than 0.5 while the uncertainties for other cases are quite large. Compared with the standard deviation of the first natural frequency, the identified second frequencies have a larger standard deviation. Almost all of them are over 2.00. As a consequence, it has larger uncertain intervals for different ice velocities. That means input parameters cause different uncertainties to modal parameters.

Table 3 shows the corresponding damping ratios of modal parameters. For the damping ratio corresponding to the first natural frequency, it is quite small (less than 0.01) for ice failure FLI. When ice failure changes to CC, it becomes larger (more than 0.018). The standard deviation is very large. It is even larger than the mean value. For example, when ice velocities are 10, 14, 16, 20, and 28 (mm/s), the large standard deviations result in unreasonable significance intervals that exceed the range of zero. This varying trend of the first damping ratio is totally different from that of the second one. It can be seen that most FLI failures generate larger damping ratios (more than 0.017) than CC failures (less than 0.014) apart from ice velocity 150 mm/s.

To sum up, the mined knowledge is listed with the following items:

(1) The poor estimation of modal parameters happens as a result of the quasi-static response of the structure in IC.
(2) For the first natural frequency, the estimated mean value is quite close to the benchmark. The standard deviation is relatively small, which renders reasonable uncertainty intervals. With the increasing ice velocities, the varying trend is not significant.
(3) For the second frequency, the bold numbers manifest that the proposed method cannot have accurate estimations for certain cases. The standard deviation shows the estimating uncertainties are very large. FLI generates larger frequencies than CC.
(4) The damping ratio of the first mode rises with the increase of ice velocity while the damping ratio of the second mode decreases from FLI to CC.

4.5. Knowledge presentation

During UA, the first straight line in the stabilization diagram is taken as the first natural frequency while the second line represents the second natural frequency. Such analysis results in a large bias to the identified parameters. For example, the first natural frequency cannot be identified by the proposed method. There is not a straight line at the position where it is supposed to appear. As a consequence, the second natural frequency is considered the first natural frequency. At the same time, the third frequency is taken as the second one. Obviously, such an assumption causes very large uncertainties in the identified parameters as shown in Tables 2 and 3.

Next, prior knowledge is used to pick up anomalies in the results. The benchmark values of the first two natural frequencies are 21.352 and 29.516 rad/s separately, which are estimated when the structure was moving in the open water (Stange et al., 2020). Considering the difference between open water and ice, the benchmark values are expanded by 10% deviation to an interval: [19.22, 23.49] for the first frequency, [26.56, 32.47] for the second frequency. The processed UA results are shown in Fig. 11 for data file 32010, Fig. 12 for data file 25010, and Fig. 13 for the full-scale measurements.

Fig. 11(a) shows the filtered first natural frequency and corresponding damping ratio. The left Y axis is the value of the identified natural frequency. The right Y axis is the corresponding damping ratio. The green dotted line represents the identified first natural frequency in Wang et al. (2022). Black points are the mean value of identified frequencies. The length of the vertical line at each point means the estimated 95% confidence interval. Based on the varying trend of

Table 2
The uncertainty analysis results of identified frequencies based on the data in '32010' under the ice failures of IC, FLI, and CC.

Frequency	Statistics	Ice velocity (mm/s)														
		4	6	8	10	12	14	16	18	20	28	45	65	80	95	150
		IC	IC	FLI	FLI	FLI	FLI	FLI	FLI	FLI	FLI	FLI	CC	CC	CC	CC
First	Mean	45.59	17.57	19.84	29.76	**21.69**	**21.02**	**21.92**	**21.06**	23.53	**21.28**	**21.59**	**21.50**	**21.25**	**21.96**	**21.81**
	Std	28.04	5.68	1.64	2.41	0.01	1.57	4.55	0.01	3.39	0.42	0.02	0.25	1.22	2.10	1.23
	Upper	102.56	28.71	23.05	26.41	21.04	24.42	30.85	21.08	30.18	22.11	21.63	21.98	23.64	26.08	24.21
	Lower	−7.38	6.44	16.63	16.97	21.00	18.28	13.00	21.05	16.88	20.47	21.55	21.02	18.85	17.84	19.40
Second	Mean	88.00	**29.73**	26.66	32.00	32.49	**29.68**	32.43	**29.01**	30.38	**29.71**	**29.32**	**29.93**	**29.42**	**29.76**	**29.57**
	Std	28.84	14.48	3.44	10.59	3.88	3.62	9.07	1.60	5.12	0.66	1.82	1.92	2.43	12.02	4.47
	Upper	144.53	58.10	33.40	52.76	40.10	36.77	50.20	32.16	40.41	31.01	32.89	33.71	34.19	53.32	38.33
	Lower	31.47	1.35	19.91	11.24	24.88	22.58	14.65	25.87	20.35	28.42	25.74	26.16	24.65	6.19	20.80

Table 3
The uncertainty analysis results of identified damping ratios based on the data in '32010' under the ice failures of IC, FLI, and CC.

Damping	Statistics	Ice velocity (mm/s)														
		4	6	8	10	12	14	16	18	20	28	45	65	80	95	150
		IC	IC	FLI	FLI	FLI	FLI	FLI	FLI	FLI	FLI	FLI	CC	CC	CC	CC
First	Mean (10^{-2})	1.41	1.30	0.31	0.24	0.09	0.10	0.29	0.08	0.78	0.04	0.64	1.86	1.24	1.73	2.03
	Std (10^{-2})	0.86	0.61	0.51	0.62	0.03	0.39	0.82	0.03	1.09	0.08	0.03	0.71	0.33	0.37	0.50
	Upper(10^{-2})	3.11	2.50	1.30	1.46	0.14	0.86	1.89	0.41	2.92	0.20	0.69	3.25	1.89	2.45	3.01
	Lower (10^{-2})	−0.28	0.10	−0.68	−0.98	0.04	−0.67	−1.31	0.03	−1.36	−0.12	0.58	0.47	0.58	1.01	1.06
Second	Mean (10^{-2})	0.70	1.70	1.74	2.12	2.84	2.32	2.45	3.00	2.43	2.41	0.86	0.73	1.15	1.31	2.20
	Std (10^{-2})	0.71	1.76	0.85	0.77	1.33	1.15	1.47	1.06	0.79	0.63	0.19	0.29	0.38	0.43	2.13
	Upper (10^{-2})	2.08	5.16	3.29	3.63	5.45	4.58	5.33	5.06	3.97	3.65	1.24	1.30	1.90	2.15	6.37
	Lower (10^{-2})	−0.69	−1.75	0.08	0.61	0.24	0.06	−0.43	0.92	0.88	1.65	0.48	0.17	0.41	0.48	−1.97

the mean value, UA has a more sensible estimation than the method without UA, especially when ice velocities are larger than 45 mm/s. The superiority can also be verified in Fig. 11(b). Overall, the first natural frequency goes up with the increase in ice velocity. This trend is the same as the damping ratio as shown by the blue line. However, this trend does not appear on the identified second natural frequency as shown in Fig. 11(b). With the increase of ice velocity, the second natural frequency goes up until velocity reaches 16 mm/s. Next, it plummets when ice velocity changes to 18 mm/s. After that, it keeps an increasing trend from 20 mm/s. The damping ratio shows an overall decreasing trend when ice moves towards higher velocity. In addition, the uncertainty of the identified second frequency and damping ratio is significantly larger than that of the first frequency and corresponding damping ratio.

Fig. 12(a) shows the significant increasing trend of the first natural frequency in data file 25010. The value rises from 19.3 to 21. For the second natural frequency, its values fluctuate vary drastically as shown in Fig. 12(b). The same trend can be found in Fig. 13. In Fig. 13(a), the value of the first natural frequency starts from 18 to 22 as the increase of ice velocity. However, there is no obvious trend of the second natural frequency in Fig. 13(b). In addition, the value of the second natural frequency is far larger than that in the data files 32010 and 25010.

The mined knowledge is summarized as follows.

(1) Compared with traditional SSI-cov, UA based on prior knowledge does have superiority regarding the accuracy of modal parameter identification. In addition, the confidence interval could provide more valuable support for the SHM.
(2) The identified first natural frequency and corresponding damping ratio present a stable upward trend with the increase of ice velocity for three different experiments. No difference between model ice and wave ice was observed in relation to that trend. A small uncertainty interval demonstrates SSI-cov and Hierarchical clustering have very good robustness for the first frequency identification.
(3) For the second frequency, its trend is not significant for all three experiments. Large uncertainty means that SSI-cov and Hierarchical clustering work worse in terms of the second frequency identification.
(4) For data files 32010 and 25010, the damping ratio of the first mode is quite small, varying within [0% 3%]. However, it becomes larger in the full-scale experiment, varying within [5% 10%].

5. Discussion

This study includes two parts. The first part is SA and the second one is UA. Both SA and UA follow the same pipeline from data sampling, SSI-cov analysis, to automated modal parameters identification. Hierarchical clustering is used for automated modal parameter identification. In this study, robust distance and Silhouette value are used to improve the accuracy of Hierarchical clustering. Meanwhile, it consumes more time. It inevitably intensifies the time cost of SA. Therefore, all parameters in the Hierarchical clustering method are fixed. Although such an assumption could cause the low accuracy of modal parameters identification, in fact, SA does not require very accurate estimation because it mainly investigates how much the variation of the model is proportioned to each input factor. If time cost could be ignored, it would be better to use robust distance and Silhouette value to obtain a more accurate estimation.

Sobol and PAWN are used for SA. Through comparison of Figs. 7 and 8, it was found that PAWN outperforms Sobol with respect to sensitivity estimation of input parameters. To be exact, PAWN is superior to Sobol under the circumstance of an equivalent sample size. If Sobol's sampling size is increased up to, for example, over 10,000, Sobol could gain a very good estimation but it is desperately time-consuming. That is because the time complexity of PAWN is $O(M \times n \times Nc)$ while Sobol's time complexity is $O(M \times N)$. Hence, considering the balance of time cost and SA accuracy, this study prefers PAWN to Sobol.

PAWN is used for SA on data files 32010, 25010, and full-scale test. From Figs. 7, 9, and 10, they show the top two influential factors are BR and SF. It can be concluded that BR and SF are the largest uncertainty sources of SSI-cov. This conclusion needs verification further using more cases. In addition, SO accounts for a relatively large sensitivity to the identified frequencies to a certain extent. This is because the identified modes are affected by the variation of SO. Nevertheless,

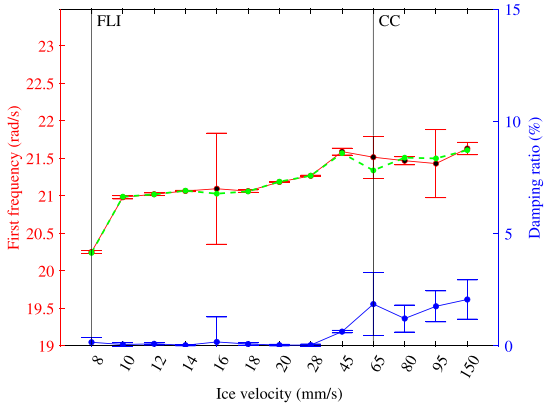

(a) First frequency and its damping ratio

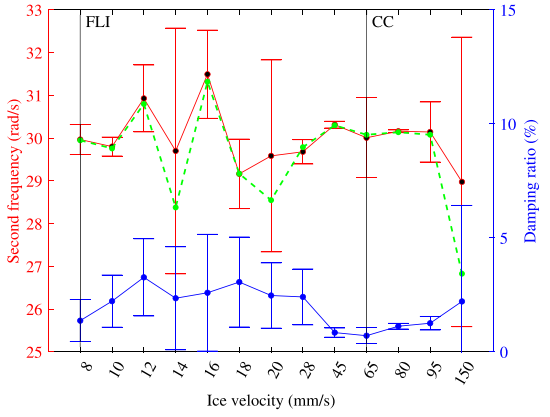

(b) Second frequency and its damping ratio

Fig. 11. The identified frequencies and corresponding damping ratios over different ice velocities in data file 32010 (Green dotted line: identified frequencies without UA; Black points: the mean value of identified frequencies; Vertical lines: 95% confidence interval.).

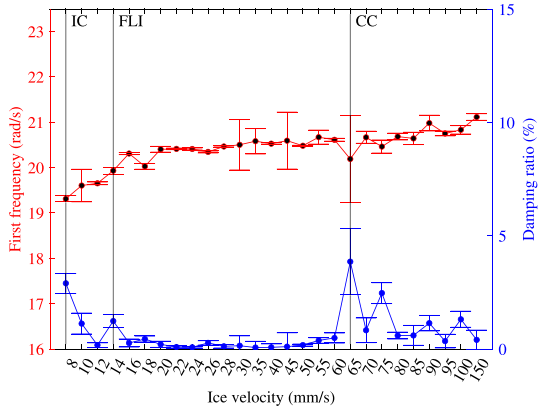

(a) First frequency and its damping ratio

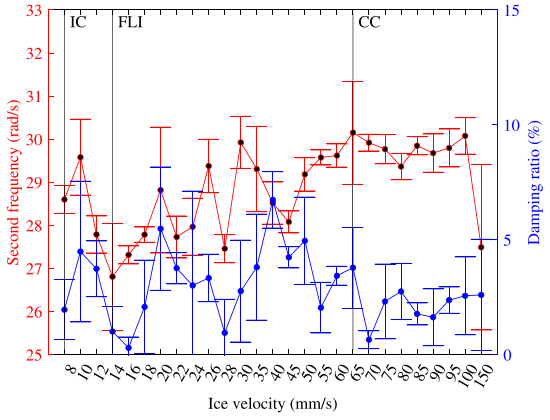

(b) Second frequency and its damping ratio

Fig. 12. The identified frequencies and corresponding damping ratios over different ice velocities in data file 25010.

when it attains a certain value, the modes are not changed with the increase of SO. Therefore, it is not considered in this study.

The same experiment settings are set for these three experiments. However, it does not work well for the full-scale test. This possibly results from less stable poles identified from the data. Therefore, in this study, we adjust the minimum size of a cluster to 5 for the full-scale data instead of 8 for the model-scale data. In addition, the benchmark interval is reset as [0,23.49] for the first natural frequency and [26.56, 50] for the second natural frequency. Such adjustments make the parameter identification more accurate for the full-scale test.

This study assumes all input parameters follow a uniform distribution instead of normal distribution. This is because sampled data from normal distribution could result in the failure of solving eigenvalues and eigenvectors. if a data point comes from a normal distribution, it might be beyond the defined range. For example, given $N(\mu, \sigma^2)$, the sampled data points would vary in $[\mu - 1.96\sigma,\ \mu + 1.96\sigma]$ rather than in $[\mu - \sigma,\ \mu + \sigma]$. Apparently, the former sampling space is larger than the later one. As a consequence, the sampled data points would exceed the rational range required by SSI-cov. In addition, in order to increase the uncertainty of the identified modal parameters, the σ is assumed as the 40% deviation of μ. if the deviation was increased, the sensitivity results would change a little bit. SA takes advantage of statistical methods to estimate the importance of factors and is subject to the impacts of many factors easily. The important parameters should be selected based on the integration of SA, expertise knowledge, and applications.

The second mode appeared difficult to identify accurately. One would expect that the second mode was easier than the first mode to identify, because it should be less influenced by the ice-failure process due to its smaller modal amplitude at the ice-action point, and therefore less nonlinearities for the SSI-cov to handle. However, due to the second mode's lower modal contribution of the global response, the signal to noise ratio for the second mode is also lower, thereby possibly inhibiting stable identifications.

6. Conclusion

The environmental variability of identified modal parameters of structures located in ice-infested waters are uncertain and to some extent unknown, therefore inhibiting efficient structural health monitoring. This study proposed a UA framework for automated modal parameter identification for structures exposed to drifting ice-conditions interaction by obtaining convincing parameters estimation with their uncertainty. The framework were composed by two parts: The first part applied an SA to picked up the most influential input variables for modal parameters' uncertainties, in which we presented a comparison between two methods for SA, namely PAWN and Sobol. PAWN was further selected for SA on ice–structure interaction data as it offered the most accurate estimation of parameters' importance. It was found that the most influential inputs to the modal parameters estimation were the number of block rows and sampling frequency. The input variables from PAWN were subsequently applied in a UA, which is the second part in Fig. 2. Here, the inputs were varied to obtain modal parameters

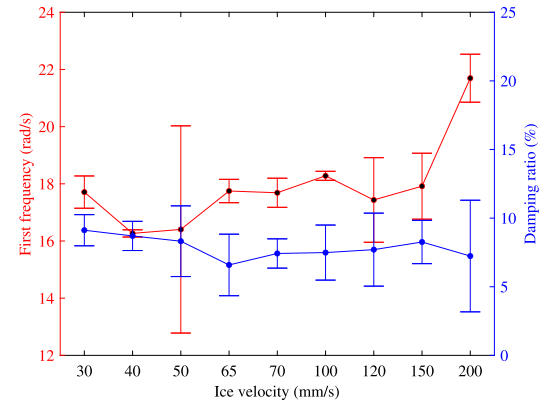

(a) First frequency and its damping ratio

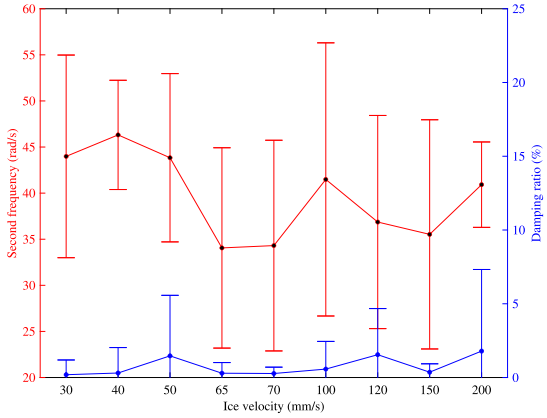

(b) Second frequency and its damping ratio

Fig. 13. The identified frequencies and corresponding damping ratios over different ice velocities in the full-scale test.

and corresponding uncertainties when applied to a covariance-driven stochastic subspace identification of modal parameters. The UA revealed significant trends in the modal parameters identified over a range of ice velocities and types of ice–structure interaction: (1) For model-scale ice–structure interaction, the first natural frequency and corresponding damping ratio arose with the increase of ice velocities (starting from frequency lock-in, and to continuous brittle crushing). Once the interaction was dominated by continuous brittle crushing, the natural frequency stabilized with further increase in ice velocity, an observation found for both model-scale and full-scale; (2) The second mode does not present a significant trend. In addition, uncertainties of the second mode (natural frequencies and damping ratios) are quite larger than those of the first mode.

The second mode appeared difficult to identify for the model-scale tests, likely due to the combination of second mode's low modal contribution of the global response and the signal to noise ratio. Future studies of environmental variability due to the presence of ice would benefit from denser sensor networks and higher sampling frequency.

CRediT authorship contribution statement

Chunlin Wang: Conceptualization, Methodology, Investigation, Writing – original draft. **Torodd Skjerve Nord:** Conceptualization, Writing – review & editing, Supervision. **Gesa Ziemer:** Review and editing, Supervision. **Guoyuan Li:** Review and editing, Supervision.

Declaration of competing interest

The authors declare that they have no known competing financial interests or personal relationships that could have appeared to influence the work reported in this paper.

Data availability

The data that has been used is confidential.

Acknowledgments

The ice model tests have been conducted as part of the FATICE project, funded under grant agreement No 728053-MarTERA. The author Chunlin Wang would like to thank the sponsorship of the Chinese Scholarship Council for funding his research at Norwegian University of Science and Technology.

References

Au, S.K., 2011. Fast Bayesian FFT method for ambient modal identification with separated modes. J. Eng. Mech. 137 (3), 214–226.
Blenkarn, K., 1970. Measurement and analysis of ice forces on cook inlet structures. In: Offshore Technology Conference. OnePetro.
Döhler, M., Mevel, L., 2013. Efficient multi-order uncertainty computation for stochastic subspace identification. Mech. Syst. Signal Process. 38 (2), 346–366.
Dusenberry, M.W., Tran, D., Choi, E., Kemp, J., Nixon, J., Jerfel, G., Heller, K., Dai, A.M., 2020. Analyzing the role of model uncertainty for electronic health records. In: Proceedings of the ACM Conference on Health, Inference, and Learning. pp. 204–213.
He, M., Liang, P., Li, J., Zhang, Y., Liu, Y., 2021. Fully automated precise operational modal identification. Eng. Struct. 234, 111988.
Helton, J.C., Davis, F.J., 2003. Latin hypercube sampling and the propagation of uncertainty in analyses of complex systems. Reliab. Eng. Syst. Saf. 81 (1), 23–69.
Hendrikse, H., Nord, T.S., 2019. Dynamic response of an offshore structure interacting with an ice floe failing in crushing. Mar. Struct. 65, 271–290.
Hu, Z., Smith, R.C., Burch, N., Hays, M., Oates, W.S., 2014. A modeling and uncertainty quantification framework for a flexible structure with macrofiber composite actuators operating in hysteretic regimes. J. Intell. Mater. Syst. Struct. 25 (2), 204–228.
Hu, Z., Smith, R.C., Ernstberger, J., 2012. The homogenized energy model for characterizing polarization and strains in hysteretic ferroelectric materials: Implementation algorithms and data-driven parameter estimation techniques. J. Intell. Mater. Syst. Struct. 23 (16), 1869–1894.
Jefferies, M.a., 1988. Dynamic response of "Molikpaq" to ice-structure interaction. In: Proceedings of the 7th OMAE, Vol. 4. Houston, February 7–12, 1988, pp. 201–220.
Kärnä, T., Andersen, H., Gürtner, A., Metrikine, A., Sodhi, D., van het Loo, M., Kuiper, G., Gibson, R., Fenz, D., Muggeridge, K., et al., 2013. Ice-induced vibrations of offshore structures-looking beyond iso 19906. In: Proceedings of the International Conference on Port and Ocean Engineering under Arctic Conditions. POAC.
Kärnä, T., Jochmann, P., 2003. Field observations on ice failure modes. In: Proceedings of the 17th International Conference on Port and Ocean Engineering under Arctic Conditions. Trondheim, Norway, June, pp. 16–19.
Kvåle, K., Øiseth, O., 2021. Automated operational modal analysis of an end-supported pontoon bridge using covariance-driven stochastic subspace identification and a density-based hierarchical clustering algorithm. In: Bridge Maintenance, Safety, Management, Life-Cycle Sustainability and Innovations. CRC Press, pp. 3041–3048.
Lauwagie, T., Van Assche, R., Van der Straeten, J., Heylen, W., 2006. A comparison of experimental, operational, and combined experimental-operational parameter estimation techniques. In: Proceedings of the International Noise and Vibration Conference. ISMA, Citeseer, pp. 2997–3006.
Li, S., Pan, J., Luo, G., Wang, J., 2020. Automatic modal parameter identification of high arch dams: feasibility verification. Earthq. Eng. Eng. Vib. 19 (4), 953–965.
Magalhaes, F., Cunha, A., Caetano, E., 2009. Online automatic identification of the modal parameters of a long span arch bridge. Mech. Syst. Signal Process. 23 (2), 316–329.
Mao, J.X., Wang, H., Fu, Y.G., Spencer, Jr., B.F., 2019. Automated modal identification using principal component and cluster analysis: Application to a long-span cable-stayed bridge. Struct. Control Health Monit. 26 (10), e2430.
Nord, T.S., 2015. Force and Response Estimation on Bottom-Founded Structures Prone to Ice-Induced Vibrations. NTNU.
Nord, T.S., Kvåle, K.A., Petersen, Ø.W., Bjerkås, M., Lourens, E.M., 2017. Operational modal analysis on a lighthouse structure subjected to ice actions. Procedia Eng. 199, 1014–1019.
Nord, T.S., Petersen, Ø.W., Hendrikse, H., 2019. Stochastic subspace identification of modal parameters during ice–structure interaction. Phil. Trans. R. Soc. A 377 (2155), 20190030.

Pan, C., Ye, X., Mei, L., 2021. Improved automatic operational modal analysis method and application to large-scale bridges. J. Bridge Eng. 26 (8), 04021051.

Pappa, R.S., James, III, G.H., Zimmerman, D.C., 1998. Autonomous modal identification of the space shuttle tail rudder. J. Spacecr. Rockets 35 (2), 163–169.

Pathmanathan, P., Cordeiro, J.M., Gray, R.A., 2019. Comprehensive uncertainty quantification and sensitivity analysis for cardiac action potential models. Front. Physiol. 10, 721.

Pianosi, F., Sarrazin, F., Wagener, T., 2015. A Matlab toolbox for global sensitivity analysis. Environ. Model. Softw. 70, 80–85.

Pianosi, F., Wagener, T., 2015. A simple and efficient method for global sensitivity analysis based on cumulative distribution functions. Environ. Model. Softw. 67, 1–11.

Rainieri, C., Fabbrocino, G., 2014. Operational modal analysis of civil engineering structures. Springer, New York 142, 143.

Razavi, S., Jakeman, A., Saltelli, A., Prieur, C., Iooss, B., Borgonovo, E., Plischke, E., Piano, S.L., Iwanaga, T., Becker, W., et al., 2021. The future of sensitivity analysis: An essential discipline for systems modeling and policy support. Environ. Model. Softw. 137, 104954.

Reynders, E., Houbrechts, J., De Roeck, G., 2012. Fully automated (operational) modal analysis. Mech. Syst. Signal Process. 29, 228–250.

Reynders, E., Pintelon, R., De Roeck, G., 2008. Uncertainty bounds on modal parameters obtained from stochastic subspace identification. Mech. Syst. Signal Process. 22 (4), 948–969.

Saltelli, A., Aleksankina, K., Becker, W., Fennell, P., Ferretti, F., Holst, N., Li, S., Wu, Q., 2019. Why so many published sensitivity analyses are false: A systematic review of sensitivity analysis practices. Environ. Model. Softw. 114, 29–39.

Saltelli, A., Ratto, M., Andres, T., Campolongo, F., Cariboni, J., Gatelli, D., Saisana, M., Tarantola, S., 2008. Global Sensitivity Analysis: The Primer. John Wiley & Sons.

Singh, S., Timco, G., Frederking, R., Jordaan, L., 1990. Tests of ice crushing on a flexible structure. In: Proc. 9th OMAE Conf., Vol. 4. Houston, pp. 89–94.

Själander, M., Jahre, M., Tufte, G., Reissmann, N., 2019. EPIC: An energy-efficient, high-performance GPGPU computing research infrastructure. arXiv:1912.05848.

Sobol, I.M., 2001. Global sensitivity indices for nonlinear mathematical models and their Monte Carlo estimates. Math. Comput. Simulation 55 (1–3), 271–280.

Stange, T., Ziemer, G., von Bock und Polach, R.U.F., 2020. Development of an experimental setup to investigate the impact of higher structural modes on dynamic ice-structure interaction. In: 25th IAHR International Symposium on Ice 2020. URL: http://hdl.handle.net/11420/8438.

Timco, G., 1991. Laboratory observations of macroscopic failure modes in freshwater ice. In: Cold Regions Engineering. ASCE, pp. 605–614.

Wang, C., Nord, T.S., Li, G., 2022. Automated modal parameters identification during ice-structure interactions. In: International Conference on Offshore Mechanics and Arctic Engineering, Vol. 85864. American Society of Mechanical Engineers, V002T02A020.

Xiao, H., Cinnella, P., 2019. Quantification of model uncertainty in RANS simulations: A review. Prog. Aerosp. Sci. 108, 1–31.

Xie, Y., Liu, P., Cai, G.P., 2016. Modal parameter identification of flexible spacecraft using the covariance-driven stochastic subspace identification (SSI-COV) method. Acta Mech. Sinica 32 (4), 710–719.

Yang, X.M., Yi, T.H., Qu, C.X., Li, H.N., Liu, H., 2019. Automated eigensystem realization algorithm for operational modal identification of bridge structures. J. Aerosp. Eng. 32 (2), 04018148.

Ye, C., Zhao, X., 2020. Automated operational modal analysis based on DBSCAN clustering. In: 2020 International Conference on Intelligent Transportation, Big Data & Smart City. ICITBS, IEEE, pp. 864–869.

Zahid, F.B., Ong, Z.C., Khoo, S.Y., 2020. A review of operational modal analysis techniques for in-service modal identification. J. Braz. Soc. Mech. Sci. Eng. 42 (8), 1–18.

Zeng, J., Hoon Kim, Y., 2021. A two-stage framework for automated operational modal identification. Struct. Infract. Eng. 1–20.

Zhang, J., Yin, J., Wang, R., 2020. Basic framework and main methods of uncertainty quantification. Math. Probl. Eng. 2020.

Ziemer, G., Stange, T., Hisette, Q., 2022. HSVA model ice–A status report. In: International Conference on Offshore Mechanics and Arctic Engineering, Vol. 85918. American Society of Mechanical Engineers, V006T07A010.